Fuel 90 (2011) 1208–1214

Contents lists available at ScienceDirect

Fuel

journal homepage: www.elsevier.com/locate/fuel

Corrosion characteristics of aluminum alloy in bio-ethanol blended gasoline fuel: Part 1. The corrosion properties of aluminum alloy in high temperature fuels

Y.H. Yoo [a], I.J. Park [a], J.G. Kim [a,*], D.H. Kwak [b], W.S. Ji [c]

[a] School of Advanced Materials Engineering, Sungkyunkwan University, 300 Chunchun-Dong, Jangan-Gu, Suwon 440-746, South Korea
[b] Research and Development Division, Hyundai-Kia Motor Company, 772-1 Jangduk-Dong, Hwasung 445-706, North Korea
[c] New Technology Development Team, NGV, 314-Dong, Seoul National University, Gwanak-Gu, Seoul 151-742, South Korea

ARTICLE INFO

Article history:
Received 15 April 2010
Received in revised form 29 October 2010
Accepted 30 October 2010
Available online 12 November 2010

Keywords:
Bio-ethanol blended fuel
Aluminum
Pitting corrosion
Alkoxide reaction

ABSTRACT

The corrosion properties of an aluminum alloy, A384, in bio-ethanol blended gasoline fuel were examined at various ethanol contents (10%, 15% and 20%) and temperatures (60, 80 and 100 °C). Localized pitting corrosion developed at a high temperature of 100 °C. The corrosiveness of the fuel increased with increasing ethanol content (E10 < E15 < E20). However, no such coincident tendency appeared for the temperature (80 < 60 < 100 °C) due to the structural change of protective hydroxide film. The overall corrosion process was characterized by both competitive factors of corrosive ethanol and a protective oxide film at a given temperature and ethanol content.

1. Introduction

Recently, bio-fuel has been promoted worldwide as an alternative energy to fossil fuel in transport applications according to the global policy to reduce greenhouse gas emissions and consumption of crude oil. Among the bio-fuels available, bio-ethanol is an attractive candidate with the advantages of a huge resource for production, simple fabrication process and the utilization of existing techniques and facilities without the need to construct new infrastructures. Moreover, bio-ethanol blended gasoline fuels can reduce the fuel cost of automotive to approximately 1–3% with increasing ethanol content by E10–E30 (ethanol vol.%) compared to regular unleaded gasoline [1–4].

The application of bio-ethanol to automotive fuels can be classified into either a gasoline additive or a substitute for gasoline [5]. In the former case, a small amount (3–25 vol.%) of bio-ethanol is blended with gasoline as a replacement for methyl tertiary butyl ether (MTBE), which is generally added as a gasoline additive at approximately 11–14% to enhance the octane number and reduce the concentration of harmful substances in the exhaust gas. The use of fossil-based MTBE has been prohibited due to the possible hazards to human health [6]. Bio-ethanol may replace MTBE with a higher octane number (~113) and lower greenhouse gas emission [7]. On the other hand, high bio-ethanol content (>85%) blended gasoline or neat bio-ethanol fuel can be used as a substitute for gasoline, which is advantageous both environmentally and for reducing the dependence on fossil fuels.

With regard to the challenge of using bio-ethanol as automotive fuel, it is important to verify the impact of this alternative fuel on the corrosion of automotive component materials. Major automotive companies in the USA, Europe, and Japan have developed flexible-fuel vehicles (FFVs), whose fuel system and engine are designed to run at any ethanol content even up to E100 fuel [2]. The components of the fuel system in FFVs are made from materials compatible with ethanol, such as stainless steel or polymer. However, as a gasoline additive, bio-ethanol blended fuel is generally used in ordinary vehicles, where the fuel system and engine are composed of light metal components, particularly aluminum alloys. In this case, aluminum alloys can corrode in the fuel mixture, resulting in a deterioration of the durability and safety of vehicles. Generally, E10 is the recommended upper bound. However, there is a paucity of reports providing specific evidence or test data on the corrosiveness of E10 [2,8]. Moreover, attempts to increase the ethanol content from E10 to E20 or higher can impose an unpredictable non-linear corrosive effect on aluminum alloys [9]. The high temperature conditions in a running vehicle engine can modify the characteristics of the ethanol-blended fuel resulting in accelerated corrosion of the aluminum alloy. Therefore, the durability and safety of fuel system components using ethanol-blended gasoline fuel should be predicted by an investigation into

* Corresponding author. Tel.: +82 31 290 7360; fax: +82 31 290 7371.
E-mail address: kimjg@skku.ac.kr (J.G. Kim).

0016-2361/$ - see front matter © 2010 Elsevier Ltd. All rights reserved.
doi:10.1016/j.fuel.2010.10.058

the corrosion characteristics of aluminum alloys along with the variables of modified fuel conditions.

This study examined the corrosion characteristics and mechanisms of the aluminum cast alloy, A384, in bio-ethanol blended gasoline fuels with different ethanol contents and temperatures, through electrochemical tests and surface analyses. In addition, the mechanisms that can cause corrosion in a high temperature ethanol-blended fuel were analyzed.

2. Material and methods

2.1. Materials

A T5 heat treated aluminum die-cast alloy, A384, which is currently used in automotive parts in contact with fuel such as cylinder blocks/head, fuel pump and delivery pipe was prepared into a $12 \times 12 \times 5$ mm rectangular shape. The major alloying elements of the alloy were silicon with a hypoeutectic composition (10.5–12 wt.%), copper (3.0–4.5 wt.%) and iron (1.3 wt.%). The actual composition of the specimen was analyzed to be 11.8, 3.2 and 1.1 wt.% for silicon, copper and iron, respectively. The detailed chemical composition is listed elsewhere [10].

The surfaces of the specimens were abraded with 600-grit SiC emery paper, rinsed ultrasonically with ethanol and finally dried with air. The preparation process for all specimens was completed within 10 min before the subsequent corrosion tests to obtain an identical condition of surface oxide film, which might affect the corrosion properties of the aluminum alloy.

2.2. Immersion tests

The corrosion medium for the immersion test was a fuel mixture of commercial unleaded gasoline and anhydrous bio-ethanol with a purity of 99.9%. Overall, nine test conditions were determined by coupling the ethanol content (10, 15 and 20 vol.%) and temperature (60, 80 and 100 °C). An autoclave was used in the immersion tests (Fig. 1) to isolate the corrosion system from the surroundings as well as to withstand the high internal pressures induced by the elevated temperatures of the fuel. The aluminum alloy specimen was exposed to the fuel under each ethanol content/temperature condition for 24 h.

2.3. Electrochemical impedance spectroscopy (EIS) measurements

The corrosion characteristics of the aluminum alloy under various fuel conditions were evaluated by EIS. Because the electrochemical tests were unavailable due to the extremely low electrolyte conductivity of the fuel, the EIS measurements were carried out in a separated electrochemical test cell after the immersion tests, as shown in Fig. 1. Although the quantitative corrosion rate in the fuel medium could not be acquired, the surface profile resulting from localized pitting corrosion damage can be analyzed using this method. The electrolyte selected for EIS measurements was a 3 wt.% Na_2SO_4 aqueous solution, which is useful for the electrochemical tests with sufficiently high conductivity but not too corrosive to aluminum by impeding the initiation of pits [11]. A 3-electrode electrochemical test cell, which was composed of the corroded specimen, high purity graphite rod and saturated calomel electrode (SCE) as the working, counter and reference electrodes, respectively, was connected to an impedance analyzer (Zahner, model IM-6e). A sinusoidal voltage of ± 10 mV was applied over the frequency range, 100 kHz–0.001 Hz. The impedance data was interpreted based on a suitable equivalent circuit, which simulates the reactions between the solution and metal surface.

2.4. Surface and solution analyses

After the immersion tests, the corroded surface, pit morphology and microstructure were observed by scanning electron microscopy (SEM) and energy dispersion spectroscopy (EDS).

3. Results

3.1. Immersion tests and EIS measurements

Fig. 2 shows the corroded surface morphology after the immersion tests for 24 h in bio-ethanol blended gasoline fuel at 100 °C. The white-colored corrosion product, $Al(OH)_3$, which covered the blackish pits was rinsed with distilled water. No corrosion damage was observed at temperatures below 100 °C. However, localized pitting corrosion developed on the surface of the aluminum alloy specimens at 100 °C, even in E10 fuel, which is the recommended

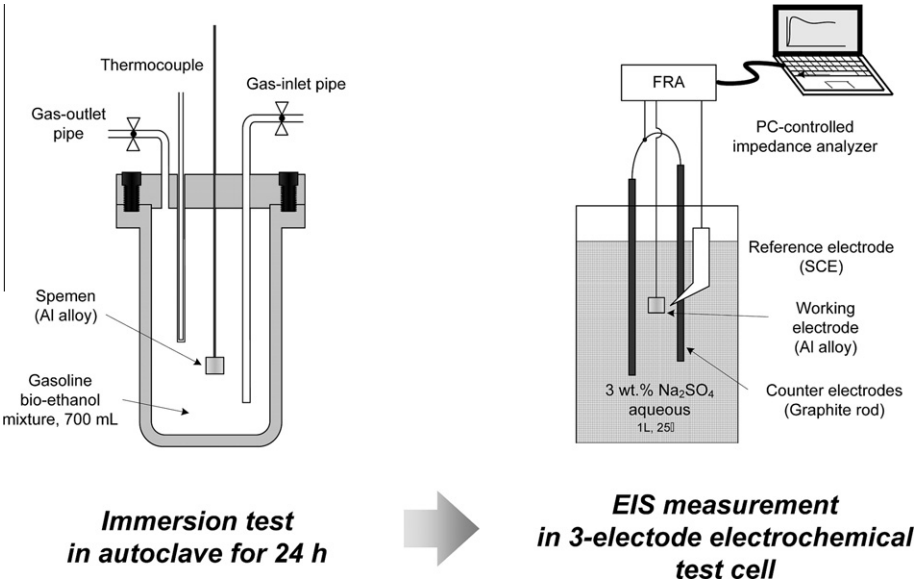

Fig. 1. Schematic diagram of the process and apparatus for the corrosion tests.

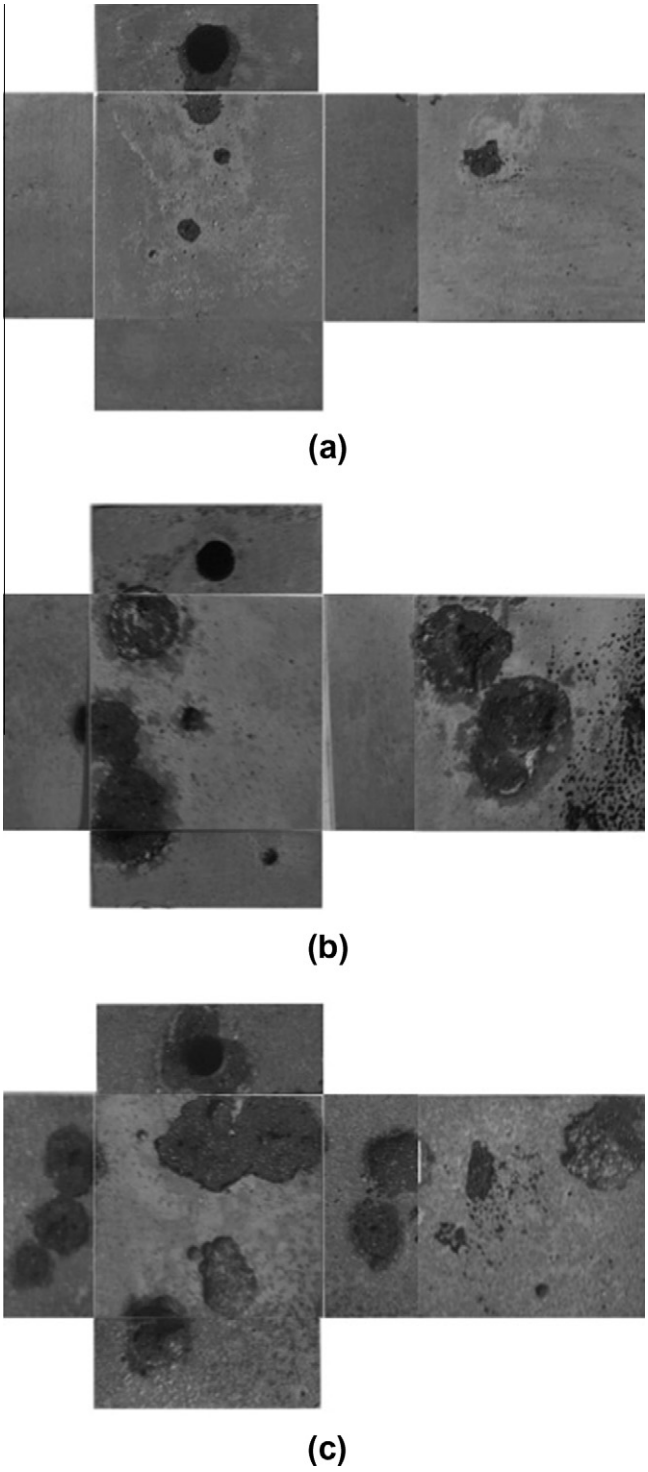

Fig. 2. The corroded surfaces of the aluminum alloy after the immersion tests at 100 °C in (a) E10, (b) E15 and (c) E20 fuel.

upper bound for ordinary vehicles. The number and dimensions of the pit increased with increasing ethanol content.

The surface profiles of the aluminum alloy that resulted from localized pitting corrosion initiated under various fuel conditions were examined by EIS. The impedance data is presented in Fig. 3 as Nyquist plots. The plots exhibited two continuous semicircles, indicating two separate interfacial reactions at the oxide film and exposed metal surface through the defects in the oxide film. The largest and smallest diameter of the Nyquist plot was observed

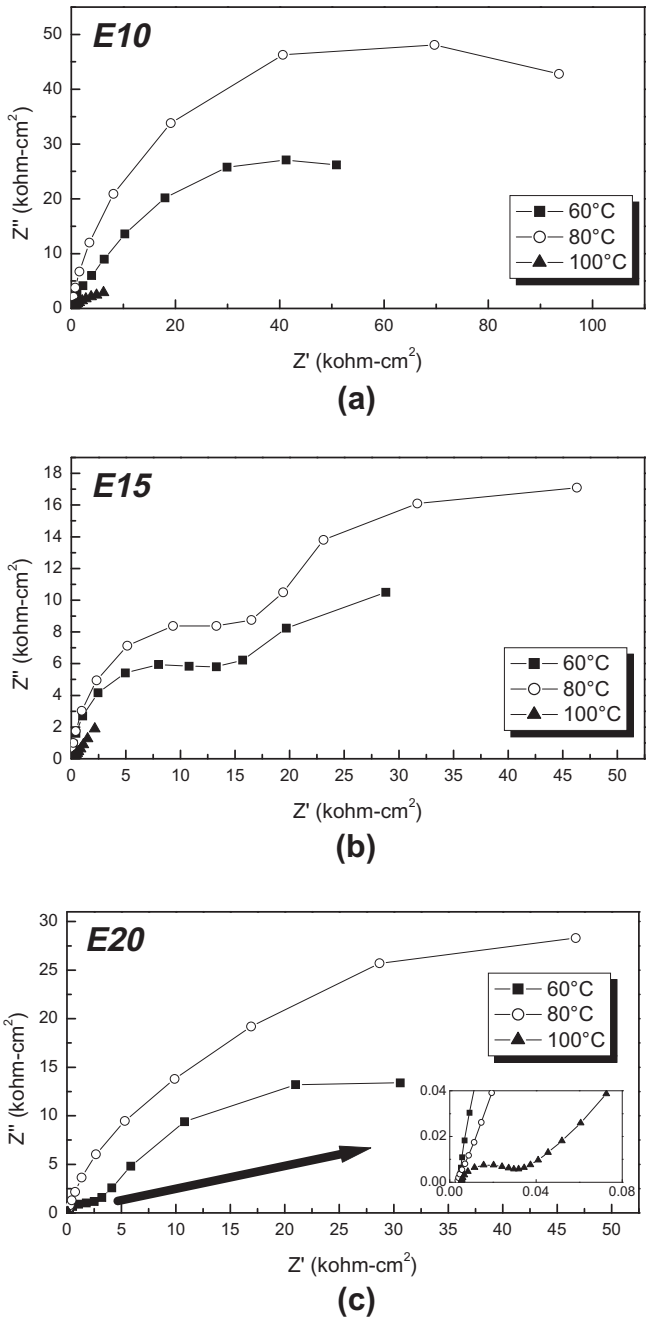

Fig. 3. Nyquist plots of the EIS measurements of the aluminum alloy after the immersion tests in (a) E10, (b) E15 and (c) E20 fuel.

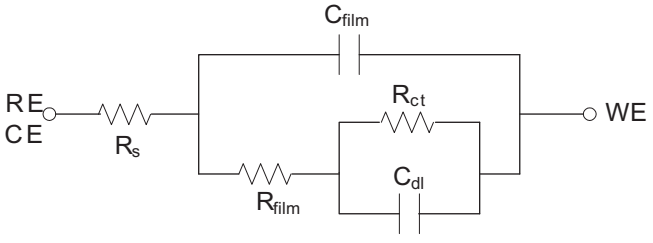

Fig. 4. Equivalent circuit for interpretation of the EIS data.

at 80 and 100 °C, respectively, at all ethanol contents. The impedance data was interpreted by fitting to the equivalent circuit presented in Fig. 4, which is typically represents to the interfacial

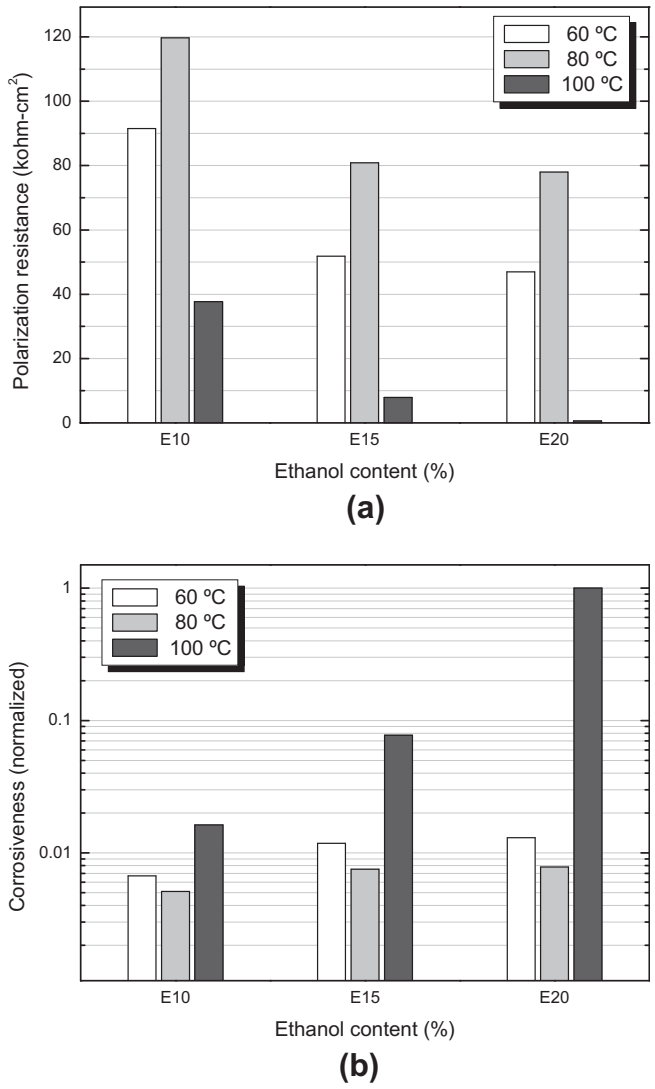

Fig. 5. Changes in (a) polarization resistance ($R_p = R_{film} + R_{ct}$) and (b) relative corrosiveness as functions of the temperature and ethanol content.

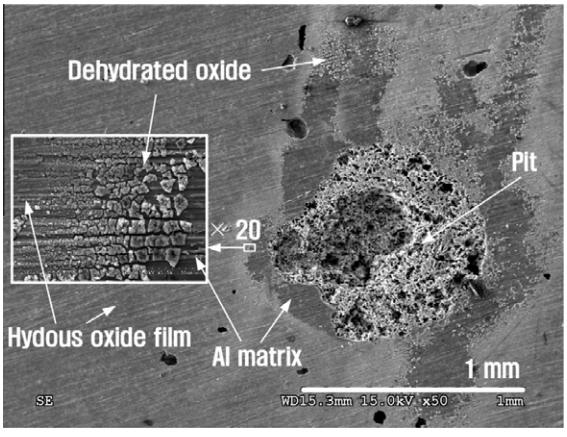

Fig. 6. Corroded surface of the aluminum alloy after the immersion test for 24 h in E10 fuel at 100 °C (SEM, 50×).

reactions with two-time constant. The equivalent circuit consisted of the following elements: R_s, the solution resistance of the test electrolyte between the working electrode and the reference electrode; C_{film}, the surface oxide film capacitance induced by dielectric behavior of the film; R_{film}, the oxide film resistance resulting from the formation of electrolytic conduction paths across the film; and C_{dl} and R_{ct}, the double layer capacitance and the charge transfer resistance between the electrolyte and metal surface within the pores, respectively.

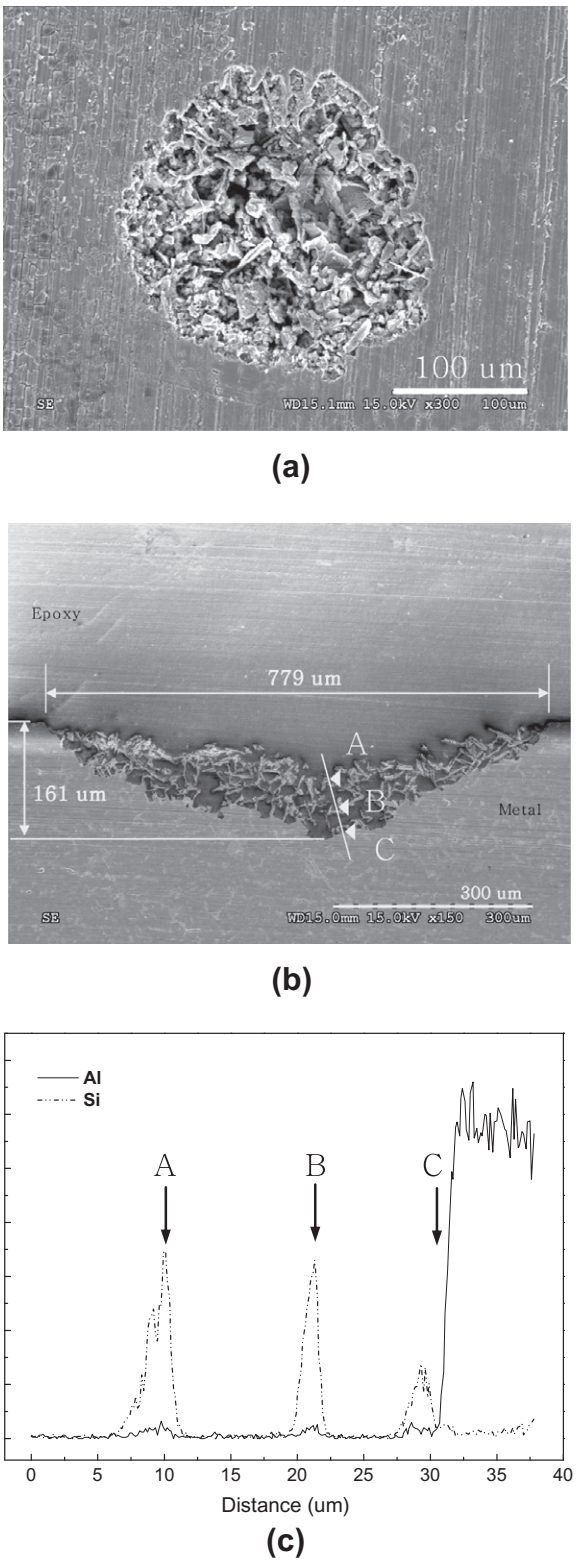

Fig. 7. Pit morphology of the aluminum alloy specimen: (a) planar view (SEM, 300×), (b) Cross-sectional view (SEM, 150×) and (c) element profiles (EDS) along with line A–C inset in (b).

The corrosion of an aluminum alloy is characterized by both the corrosion of the metal itself and the properties of the protective oxide. Accordingly, the polarization resistance (R_p), which is the summation of R_{film} and R_{ct}, was used to determine the corrosion properties as a function of the ethanol content and temperature of the ethanol-blended fuel, as shown in Fig. 5(a). R_p of the aluminum alloy decreased drastically in the range from E10 to E15, and then, decreased gradually from E15 to E20. Regarding temperature, R_p exhibited the highest value at 80 °C, and decreased drastically with further increasing temperature where pitting corrosion occurred. The relative corrosiveness of the fuel condition at various temperatures and ethanol contents were compared by calculating the ratio of the reciprocal R_p value at each temperature–ethanol content condition to that of the lowest R_p at E20-100 °C, as shown in Fig. 5(b). The corrosiveness increased with increasing ethanol content (E20 > E15 > E10), and temperature (100 > 60 > 80 °C), respectively.

3.2. Surface analyses

Fig. 6 shows a SEM image of the corroded surface of the aluminum alloy after the immersion test in the E10-100 °C fuel. A hydrous oxide film formed homogeneously in the intact region, whereas it ruptured and the aluminum matrix was exposed in the vicinity of the pit. In the boundary, the oxide film was dehydrated, exhibiting multiple cracks. These cracks were attributed to the relaxation of tensile stress induced by volume shrinkage of the oxide film during the dehydration reaction [12], causing the exfoliation of oxide fragments in the vicinity of the pit due to the turbulence of the product gas or other fluid during the corrosion reactions in the pit.

Fig. 7 shows the pit morphology and elemental profiles of the aluminum alloy observed by SEM and EDS after the immersion test in the E20-100 °C fuel. The pit propagated with a wide and shallow shape and the internal shape had a sharp and porous structure, which was occupied mainly by a platelet silicon phase, as shown in Fig. 7(c). In addition to silicon, a small amount of alloying element, such as copper and iron, were detected, which precipitated to Al_2Cu, Al_3Fe and α-AlFeSi phases in the A384 alloy during heat treatment. An identical shape of the pit was observed on the alloys immersed in the fuel at all ethanol contents. The lack of aluminum in the pit inside suggests that the corrosion reaction was accompanied by selective dissolution of the aluminum matrix, leaving the original structure of the eutectic silicon phase and precipitates.

4. Discussion

The major mechanism for the corrosion of aluminum in ethanol-blended gasoline fuel is the phase separation theory [8,13–17]. According to this theory, the hydrophilic property of ethanol allows water to be included in the fuel, which facilitates dividing the single phase ethanol–gasoline mixture into two phases of water–ethanol and gasoline. As a result, the separated water–ethanol phase causes the metal to corrode. However, phase separation itself cannot explain the corrosion in ethanol-blended gasoline fuel at high temperatures because the probability of phase separation decreases significantly with increasing temperature, even up to 60 °C, due to the increasing water tolerance for a single phase fuel mixture [16,17]. Therefore, another possible mechanism for the corrosion process was examined with respect to the chemical reaction between aluminum and ethanol, and the protective properties of the surface oxide film, as a function of temperature.

4.1. Corrosion reaction between aluminum alloy and ethanol in fuel

Aluminum in contact with ethanol can be dissolved by the chemical reaction shown below.

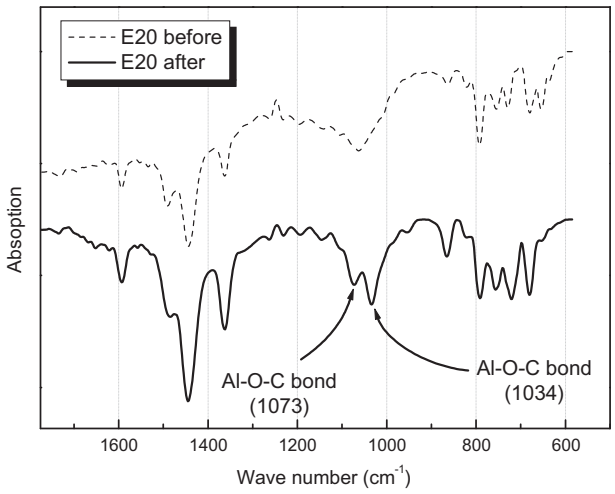

Fig. 8. FT-IR spectrum of the E20 fuel sampled before and after the immersion test.

$$3C_2H_5OH + Al \rightarrow 3/2H_2 + Al(C_2H_5O)_3 \quad (1)$$

In this reaction, an organic metal compound, aluminum alkoxide (or alcoholate), and hydrogen gas are produced by substituting a hydrogen atom in the OH group of ethanol for an aluminum atom in the metal or oxide film. The compound exists as colloidal manner with high viscosity and is soluble in the medium. Therefore, aluminum is no longer protected and will be attacked continuously [18].

To confirm the aluminum alkoxide reaction in the corrosion process, the corrosion products dissolved in the ethanol-blended fuel were analyzed after the immersion test. Fig. 8 shows the results of FT-IR analyses for the E20 fuel sampled before and after the immersion test at 100 °C. Two distinct peaks observed at 1034 and 1073 cm^{-1} were assigned to Al–O–C bonding in the spectra after the immersion test, which corresponds to aluminum isopropoxide and aluminum 2-pentoxide as a type of aluminum alkoxide, respectively [19]. The aluminum alkoxides dissolved in the fuel confirmed that a chemical reaction between aluminum and ethanol is the key process in the corrosion reaction, which causes the selective dissolution of aluminum in the pit.

Additional evidence for the aluminum alkoxide reaction was provided by the dehydration of the oxide film near the pit shown in Fig. 6. The aluminum alkoxides produced by the corrosion reaction accumulated in the pit region. These colloidal corrosion products could be transformed to white-colored $Al(OH)_3$, which covered the pit by hydrolysis via the reaction shown in Eq. (2) [20].

$$Al(C_2H_5O)_3 + 3H_2O \rightarrow Al(OH)_3 + 3C_2H_5OH \quad (2)$$

The extraction of water from the hydrous oxide film should occur either by the hydrolysis of aluminum alkoxide or the affinity of the ethanol by-product for water in Eq. (2). Although it is unclear which is dominant, dehydration of the hydrous oxide film should be induced by the aluminum alkoxide that formed during the corrosion process according to Eq. (1).

The kinetics of the aluminum alkoxide reaction as a function of temperature was examined by the weight change in the aluminum alloy specimen after the immersion tests in E20 for 12 h at 60, 80 and 100 °C. In these immersion tests, the dissolved oxygen in the fuel was removed by bubbling with nitrogen gas for 2 h before heating to examine the activity of the aluminum alkoxide reaction, excluding the protective effect of the oxide film, which should be promoted by oxygen. The specimens immersed in the oxygen-free E20 fuel showed severer corrosion damage at 80 °C and 100 °C than those immersed in ambient E20 fuel presented in

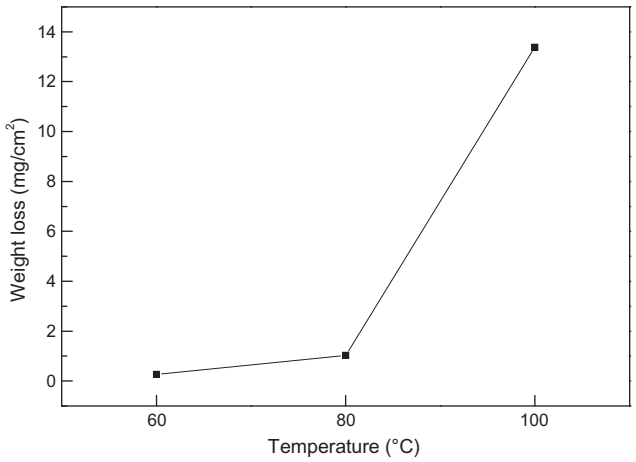

Fig. 9. Weight loss of the aluminum alloy after the immersion tests in oxygen-free E20 fuel for 12 h.

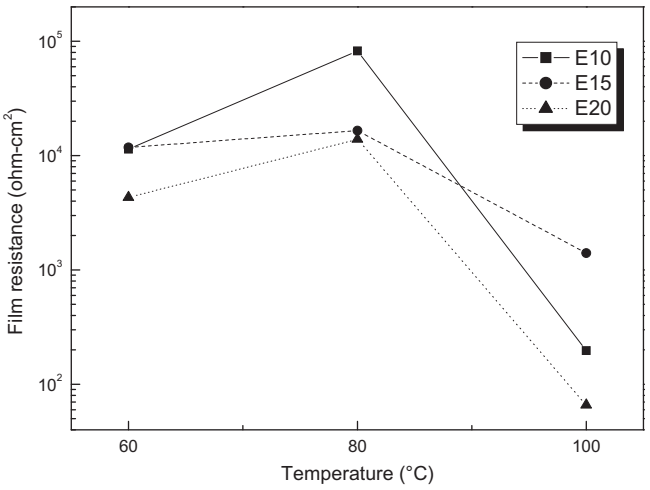

Fig. 10. Oxide film resistance of the aluminum alloy obtained from EIS analyses.

Section 3.1, even though the immersion time was shorter. On the other hand, no corrosion damage was observed in the specimen immersed at 60 °C, which is the same as the result of the immersion test in ambient E20 fuel. Fig. 9 shows the weight loss of the aluminum alloy specimen after the immersion tests in oxygen-free E20 fuel at different temperatures. A slight increase in weight loss was observed up to 80 °C, which increased significantly between 80 and 100 °C. This indicates that the aluminum alkoxide reaction is thermally activated remarkably at the temperature range above 80 °C. On the contrary, the reaction is not so activated at temperature below 80 °C.

4.2. Property of protective surface film as a function of temperature

The corrosion of an aluminum alloy might be affected by the reactions of the surface oxide film with water, which possibly enter the fuel as an impurity during handling or storage, or as a by-product from the oxidation of ethanol [18,21].

The oxide film hydrated in contact with the water has a different structure depending on the temperature [18,22]. At temperature range, 60–80 °C, the oxide film grows in three stages [22]: (1) growth of an amorphous film formed at the time of immersion (2) growth and transformation of the amorphous film into crystalline aluminum oxyhydroxide (boehmite, AlOOH), and (3) formation of aluminum hydroxide (bayerite, $Al(OH)_3$) at the external surface. The time required for these stages depends on the temperature and a final aluminum hydroxide layer is formed within 5 h at 60 °C. On the other hand, above this temperature range, the increased mobility of reacting ions due to the sufficient thermal energy allows the ions to arrange the preferential orientation of crystal aluminum oxyhydroxide growth so that the aluminum oxyhydroxide grows continuously without the stage of (3). The surface film grown to aluminum oxyhydroxide is more protective than the aluminum hydroxide film and offers further protection by thickening with increasing temperature [18].

Fig. 10 shows the R_{film} obtained from EIS analyses of the Nyquist plots in Fig 3. The result of increasing R_{film} between 60 and 80 °C confirmed that the aluminum oxyhydroxide film formed at 80 °C has superior protective ability to the aluminum hydroxide film formed at 60 °C. Although the protective ability of the oxyhydroxide film itself should increase due to thickening at further elevated temperatures, R_{film} decreased drastically at 100 °C due to pitting corrosion affected by other thermally activated corrosion mechanisms.

Overall, ethanol and a surface film of aluminum act as a primary corrosive and a protective factor, respectively, depending on the temperature. The overall corrosion process that shows non-proportional behavior as a function of temperature in Fig. 5(b) is characterized by the competitive results between these two factors. The protective factor of the hydrous oxide film which is dominant at lower temperatures (60–80 °C) led to a decrease in corrosiveness, whereas the corrosive factor of the aluminum alkoxide reaction, which is dominant at the temperatures over 80 °C led to an exponential increase in that of aluminum alloy in the bio-ethanol blended fuel.

5. Conclusions

The corrosion properties of an aluminum alloy, A384, in bio-ethanol blended gasoline fuel with different ethanol contents were examined at various elevated temperatures. Localized pitting corrosion developed on the surface of the aluminum alloy after the immersion tests at 100 °C for 24 h regardless of the ethanol content. The number and dimensions of the pits increased with increasing ethanol content from E10 to E20. No corrosion damage was observed below 100 °C. The corrosiveness calculated from the EIS measurements increased with increasing ethanol content (E10 < E15 < E20) but there was no such tendency with increasing temperature (80 < 60 < 100 °C). This was attributed to the temperature-dependent formation of hydrous oxide film, i.e., aluminum hydroxide film at 60 °C and the more protective aluminum oxyhydroxide film at 80 °C. A thermally activated chemical reaction between aluminum and ethanol was found to be the key process in the aluminum corrosion in the high temperature ethanol-blended fuel from the result of aluminum alkoxide formation. Consequently, the overall corrosion process of the aluminum alloy in ethanol-blended gasoline fuel is characterized by the competitive factors of a protective surface oxide film, which dominates at temperatures between 60 and 80 °C, and corrosive ethanol, which is activated at the temperature above 80 °C.

References

[1] Charles MB, Ryan R, Ryan N, Oloruntoba R. Public policy and biofuels: the way forward? Energy Policy 2007;35:5737–46.
[2] Yacobucci BD, Schnepf R. Selected issues related to an expansion of the renewable fuel standard (RFS). CRS report for Congress (US): Congressional Research Service; 2008. Report No.: RL34265.
[3] Hoekman SK. Biofuels in the U.S. – challenges and opportunities. Renewable Energy 2009;34:14–22.
[4] American coalition for ethanol. Fuel economy study. Sioux Falls (SD): American coalition for ethanol; 2005.
[5] Szklo A, Schaeffer R, Delgado F. Can one say ethanol is a real threat to gasoline? Energy Policy 2007;35:5411–21.

[6] Menezes EW, Cataluña R, Samios D, Silva R. Addition of an azeotropic ETBE/ethanol mixture in eurosuper-type gasolines. Fuel 2006;85:2567–77.
[7] Biomass program: ethanol myths and facts [Internet]. Washington: Energy Efficiency and Renewable Energy (EERE), US Department of Energy. Available from: http://www1.eere.energy.gov/biomass/ethanol_myths_facts.html. (accessed 29.09.09).
[8] Orbital Engine Company. A literature review based assessment on the impacts of a 10% and 20% ethanol gasoline fuel blend on non-automotive engines. Report to Environment Australia; 2002.
[9] Jones B, Mead G, Steevens P, Timanus M. (Minnesota Center for Automotive Research at Minnesota State University, Mankato, MN). The effect of E20 on metals used in automotive fuel system components. St. Paul (MN): Minnesota Department of Agriculture; 2008. Report No.: 2-22-2008.
[10] Cayless RBC. Alloy and temper designation systems for aluminum and aluminum alloys. In: Metals handbook. Properties and selection: nonferrous alloys and special-purpose materials, vol. 2. Ohio: ASM International; 1990. p. 15–28.
[11] Chung MK, Choi YS, Kim JG, Kim YM, Lee JC. Effect of the number of ECAP pass time on the electrochemical properties of 1050 Al alloys. Mater Sci Eng A 2004;366:282–91.
[12] Geiculescu AC, Strange T. A microstructural investigation of low-temperature crystalline alumina films grown on aluminum. Thin Solid Films 2003;426:160–71.
[13] Westbrook PA. Compatibility and permeability of oxygenated fuels to materials in underground storage and dispensing equipment in oxygenate compatibility and permeability report. California State Water Resources Control Board (CA); 1999.
[14] French R, Malone P. Phase equilibria of ethanol fuel blends. Fluid Phase Equilib 2005;228–229:27–40.
[15] Oak Ridge National Laboratory. Ethanol pipeline corrosion literature study. Final report. Oak Ridge (TN): United States Government (US); 2008.
[16] Filho OV (Delphi South America technical center, Brazil). Gasoline C made with hydrous ethanol. HE Blends BV; 2008.
[17] Letcher TM, Heyward C, Wootton S, Shuttleworth B. Ternary phase diagrams for gasoline–water–alcohol mixtures. Fuel 1986;65:891–4.
[18] Vargel C. Corrosion of aluminum. Oxford: Elsevier Ltd.; 2004.
[19] Guertin DL, Wiberley SE, Bauer WH, Goldenson J. The infrared spectra of three aluminum alkoxides. J Phys Chem 1956;60:1018–9.
[20] Scholz M, Ellermeier J. Corrosion behavior of different aluminum alloys in fuels containing ethanol under increased temperatures. Mat -wiss U Werkstofftech 2006;37:842–51.
[21] Marinov N. A detailed chemical kinetic model for ethanol oxidation. Int J Chem Kinet 1999;31:183–220.
[22] Hart RK. The formation of films on aluminum immersed in water. Trans Faraday Soc 1957;53:1020–7.